S03120100-TRT10012
ORNL/TM-2023/3215

# Oak Ridge National Laboratory Methodology to Generate Decay Gamma Sources for the Second Target Station Full Target Assembly

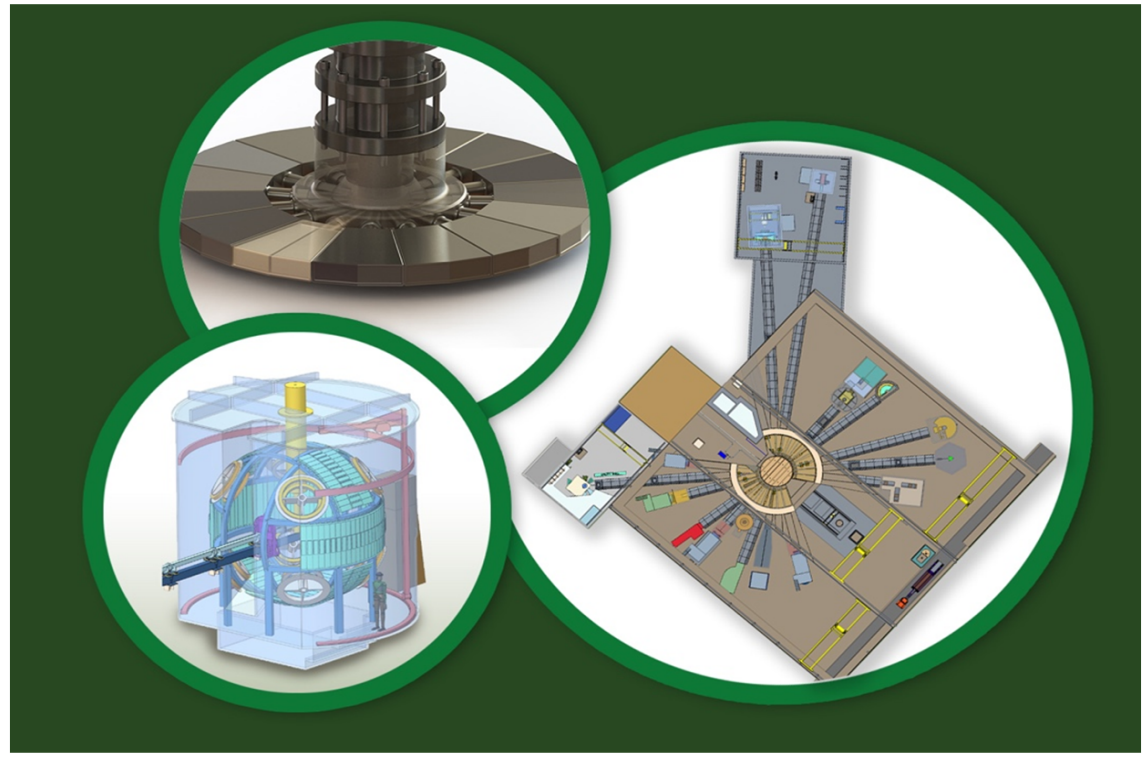

Tucker McClanahan, Ph.D.

**April 2024**



OAK RIDGE National Laboratory

ORNL IS MANAGED BY UT-BATTELLE LLC FOR THE US DEPARTMENT OF ENERGY

**S03120100-TRT10012**
**ORNL/TM-2023/3215**

Second Target Station Project

# Methodology to Generate Decay Gamma Sources for the Second Target Station Full Target Assembly

Tucker McClanahan, Ph.D.

April 2024

Prepared by
OAK RIDGE NATIONAL LABORATORY
Oak Ridge, TN 37831
managed by
UT-Battelle LLC
for the
US DEPARTMENT OF ENERGY
under contract DE-AC05-00OR22725

# CONTENTS

## LIST OF FIGURES

## LIST OF TABLES

## ABBREVIATIONS

| | |
|---|---|
| ORNL | Oak Ridge National Laboratory |
| STS | Second Target Station |

# 1 SCOPE

This report details the specifics of applying the *Position-Averaged Method* to the target wedges and staves. The methodology used to calculate the decay gamma sources for a single target wedge to the calculation of the Second Target Station (STS) target assembly activation and the resulting decay gamma source terms are detailed in this report [1, 2]. The methodology has been applied to the entire STS target assembly including all of the target wedges, staves, shaft, and drive. The target staves and shaft have been vertically segmented to ensure the decay gamma source gradient is sufficiently captured. MCNP® Code Version 6.2.0 with the RNUCS patch coupled with CINDER2008 from the AARE V1.0 package are the main tools used to calculate the decay gamma source terms [3, 4, 5].

## 2 ACCEPTANCE CRITERIA

Not Applicable

## 3 ASSUMPTIONS AND LIMITATIONS

The main assumptions associated with the transmutation methodology are detailed in earlier reports [1, 2]. The decay gamma sources are for the target wedges and staves after 10 years of operation and 8 hours, 1 week, and 2 weeks of decay after last beam on target, and after 40 years of operation for the target shaft and drive with the same decay times. An operational year is defined as 2500 hr beam-on, 1880 hr beam-off, 2500 hr beam-on, and 1880 hr beam-off.

## 4 METHODOLOGY AND MODELS

The target assembly decay gamma sources use the same methodology detailed in McClanahan's report applying the *Position-Averaged Method* to the target wedges and staves, and normal activation techniques to the shaft and drive [2]. Figure 1 shows the overall method for calculating decay gamma sources. ADVANTG 3.2.0 is first used to generate weight windows to achieve variance reduction in the subsequent MCNP® transport calculation. Section 4.1 describes the geometry used in both ADVANTG to generate weight windows as discussed in Section 4.4 and MCNP® to calculate neutron fluxes and spallation products production and destruction rates. The materials with appropriate impurities are discussed in Section 4.2. MCNP® is used to transport the proton beam discussed in Section 4.3 with the physics options discussed in Section 4.5 in order to calculate the neutron fluxes and spallation products in the target assembly. The details of the tallies used to tally the neutron fluxes are discussed in Section 4.6. Section 4.7 discusses the details of the transmutation calculations done with CINDER2008 and the accompanying scripts from the AARE package. Section 4.8 discusses how the results from the transmutation calculation are post processed.

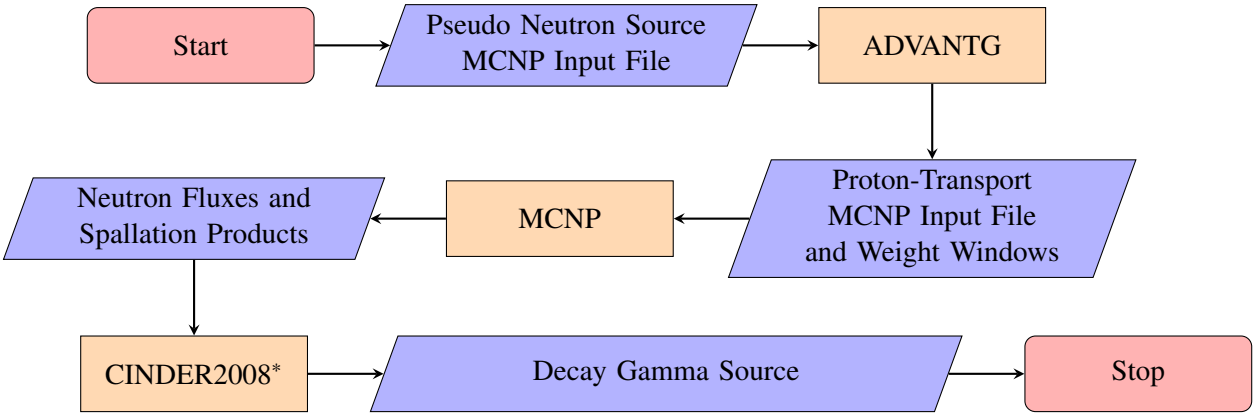


**Figure 1. R2S Transmutation Workflow where the CINDER2008* refers to using the *Position-Averaged Method* [2].**

## 4.1 GEOMETRY

The full STS facility model from the target out to the outside of the bunker is used during the weight window generation and proton transport calculations. An overview of the geometry is shown in Figure 2 where the starting proton beam location is shown as a red star, and various assemblies are labeled. Appendix C contains more figures of the geometry.

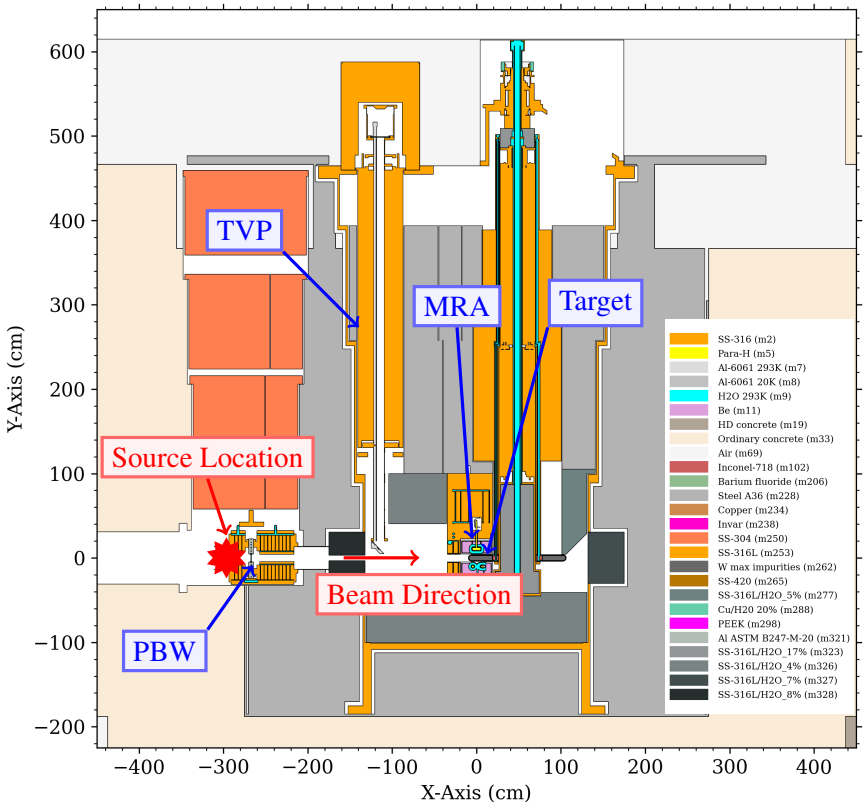


**Figure 2. Overview of the geometry used to calculate neutron fluxes and spallation products in the target wedge.**

## 4.2 MATERIALS

The materials used in support of the study are included in Appendix D. Impurities from STS material specifications from the lead engineers are included in the materials in Appendix D. The HILO-2K multi-group library is used in the weight-window generation, ENDF/B-VII.1 continuous energy cross sections are used in the initial proton beam transport, and the 321 energy group flat-weighted CINDER2008 cross section library is used during the transmutation [6]. Each material card must be accompanied by a material card nuclide substitution card (*mx*) for deuteron, triton, hellion, and alpha particles specifying the keyword “model” for each nuclide on the material card. By including these *mx* cards, all of the interactions between the specified particles and the materials will be handled by the physics models and the products of the interactions will be captured by the *rnucs* print out.

### 4.3 PROTON SOURCE

The high-fidelity proton source used in the initial neutron flux and spallation product calculation starts 300 cm upstream of the outermost surface of the target, just upstream of the proton beam window. The spatial distribution is constructed by sampling the original proton beam profile as created for the quadrapole magnet configuration by the accelerator systems analysis and converting the sampling into a MCNP®-compatible source by Wouter de Wet. In order to use the sampled data, MCNP® has been patched to load in a *source_arrays.txt* file with the sampled proton beam data and properly sample the location, direction, and energy of the proton history. The *source_arrays.txt* file used in this simulation was *qd60_sampled_source_d_0300_cm_source_arrays.txt*.

The spatial profile of the source is shown in Figure 3 and 95% of the beam falls within an area of 62.5 $cm^2$ on the face of the target. The proton energy is 1.3 GeV, the proton beam power is 0.7 MW, and arrives on target in pulses at a 15 Hz repetition rate resulting in a source strength of $3.3611 \times 10^{15}$ protons per second. The proton transport run calculates the neutron fluxes and spallation products with a source weight of 1.0. The source strength normalization of $3.3611 \times 10^{15}$ protons per second is applied during the transmutation step of the calculation as discussed in Section 4.7.

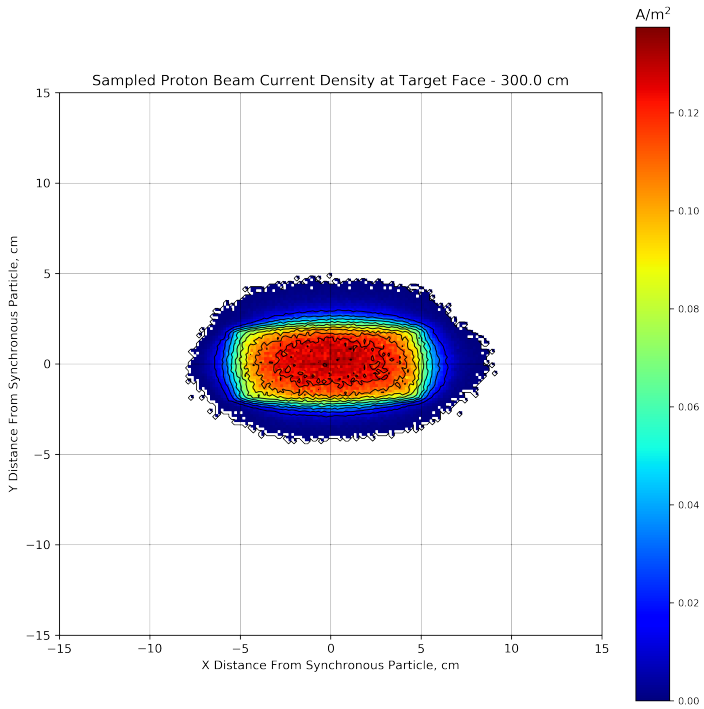


**Figure 3. Proton source spatial distribution at the target face courtesy of Wouter de Wet.**

### 4.4 VARIANCE REDUCTION

ADVANTG 3.2.0 was used to produce variance reduction parameters in the form of weight windows to aid in the timely convergence of the tallies discussed in Section 4.6. ADVANTG 3.2.0 is strictly limited to neutral particles and a surrogate neutron source was used to generate the weight window parameters in accordance with the methods provided in Miller's article [7]. In order to construct the surrogate neutron source, a structured mesh-based neutron tally that was binned in energy was placed over the entire target wheel. This mesh-based tally was then post-processed into an ADVANTG-compatible source that had the proper spatial and energy dependence of the true source but approximated the angular component of the source as isotropic. The tally-of-interest in the ADVANTG run included all cells in all 20 target segments. The quadrature set used in the ADVANTG run was generated by Joel Risner and was a midpoint gauss quadrature set with 26 polar angles and 166 total angles per octant based on quadrature studies carried out by I.K. Abu-Sumays [8].

### 4.5 PHYSICS OPTIONS

Table 1 shows the various data cards related to controlling the physics processes MCNP® uses during the proton beam to target calculation. Descriptions of the options are also included in the table. The cards shown in Table 1 were selected due to the relevance to proper high-energy activation calculations for the STS.

**Table 1. Physics Card Options for Activation Calculations**

| Card | Options | Description |
|---|---|---|
| *mode* | n p \| h ! / z k % ^ d t s a * ? | Include all relevant particles |
| *phys:n* | 1400 6j 20 | Set the cutoff energy to 1400 MeV and the transition from cross section tables to physics models to 20 MeV |
| *phys:p* | 1400 2j -1 | Set the cutoff energy to 1400 MeV and photonuclear physics to on but unbiased |
| *phys:h* | 1400 j 1 | Set the cutoff energy to 1400 MeV and the transition from cross section tables to physics models to 1 MeV |
| *phys:/* | 1400 | Set the cutoff energy to 1400 MeV |
| *lca* | 2 1 1 0023 1 1 0 1 1 0 66 | Use the default CEM 3.03 model |
| *lcb* | 3.49E+03 3.49E+03 2.49E+03 2.49E+03 8.0E+02 8.0E+02 -1 -1 | Using the defaults |
| *lea* | 1 4 1 0 1 0 0 1 | Using the defaults |
| *leb* | 1.5000E+00 8.0000E+00 1.5000E+00 1.0000E+01 | Using the defaults |
| *rnucs* | cinder normal | Invoking the print out of all spallation product rates for all cells using the normal sampling method. |
| *csize* | | Invoking the print out of all the cells bounding boxes |

## 4.6 TALLY DETAILS

Volume-averaged neutron flux tallies are used to tally the neutron fluxes in each cell of the target assembly in the MCNP® protons-on-target transport calculation. These tallies are binned in energy with the same 321-bin structure as the CINDER2008 flat-weighted cross section data and is shown in Appendix E. By binning with 321 energy groups, the resonance-effects of the cross sections are sufficiently captured, and result in accurate activation quantities.

## 4.7 TRANSMUTATION

This section outlines the details of the transmutation mechanics used to compute the decay gamma spectra. Figure 1 shows the rigorous two-step (R2S) method used to calculate the radionuclide inventories. The R2S method begins by utilizing MCNP® to transport the proton source and tally the neutron fluxes and spallation products in the regions of interest using the variance reduction parameters generated by ADVANTG. These neutron fluxes and spallation products are fed into CINDER2008 to produce radionuclide inventories and decay gamma sources for three decay time steps following 10 years of operation: 8 hours, 1 week, and 2 weeks for the target wedges and staves. The target shaft and drive decay gamma source terms were calculated for 40 years of operation with 8 hours, 1 week, and 2 weeks of decay. One operating year is assumed to consist of two sets of beam on and beam off, where a set is 2500 hr beam on and 1880 hr beam off.

The *Position-Averaged Method* described in ORNL/TM-2022/2639 is used as the basis to calculate the radionuclide inventory in the target wedges and staves [1]. A slight modification in the *Position-Averaged Method* was implemented in the transmutation method used in this report. The full source strength was used on the sum of all neutron fluxes and spallation products in like cells in all 20 target wedges. For example, in order to calculate the activation of the first tungsten layer, all of the neutron fluxes and spallation product rates are summed and the full normalization of $3.3611\times10^{15}$ protons per second is applied to the activation calculation. The resulting decay gamma spectra is then divided by the number of target wedges (20) resulting in the decay gamma spectra for each individual target wedge and stave.

## 4.8 POST PROCESSING

The resulting decay gamma spectra from Section 4.7 are then processed by the AARE_GAMMA_SOURCE_SCRIPT and a python script that utilizes the ACTIUM Python Toolkit [9]. The python script produces MCNP® *sdef* cards in vertical format and ensures no zero probability cells are present in the card. The python script also generates *sdef* cards that are compatible with ADVANTG that have been split up so that range of source intensities included in the *sdef* card does not exceed a factor of 100. The need for the splitting of the *sdef* cards is due to the limitations of ADVANTG. ADVANTG ignores the source biasing parameters supplied on the beginning *sdef* cards. By ignoring the biasing parameters, cells with relatively low source intensity are not sampled, and therefore are not included in the ADVANTG source term to generate weight windows for the decay photon transport calculation. ADVANTG not sampling those low intensity sources results in weight windows that allow high-weight histories to contribute to the tallies of interest and increase the variance in the tallies. These *sdef* cards are discussed in Section 5.

The geometry and source intensity plots are generated using the RTPlotter Python suite of tools developed by Joel Risner.

## 5 ANALYSIS AND RESULTS

This section details the decay gamma spectra calculated with the methods and tools described above. Figures 4, 5 & 6 show the decay gamma source for the lower portion of the target assembly after 8 hours, 1 week, and 2 weeks of decay. Appendix F contains several other figures of the target assembly gamma sources after 8 hours, 1 week, and 2 weeks of decay.

The attached *target_assembly_gamma_sources.tar.gz.txt* contains all of the decay gamma sources for the target assembly. The *.tar.gz.txt* file electronically attached to this document are available by using a PDF viewer that supports PDF attachment such as Adobe Acrobat, Adobe Reader, Firefox etc. Each text file in the *.tar.gz.txt* file contains decay gamma spectra for every decay time. Once the reader downloads the *.tar.gz.txt* file, the reader must delete the *.txt* from the filename before opening the *.tar.gz* file. The sources with "advantg" in the name of the file are compatible with ADVANTG for generation of weight windows for a decay gamma transport calculation.

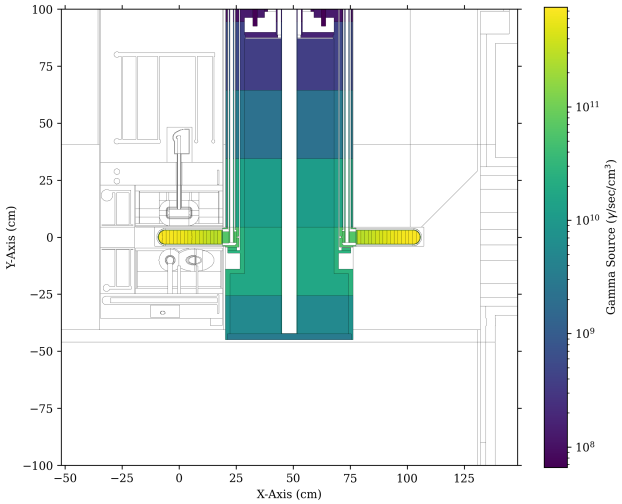


**Figure 4. Cross section view of the 8 hour decay gamma source intensity for the target wedges and lower portions of the staves and shaft.**

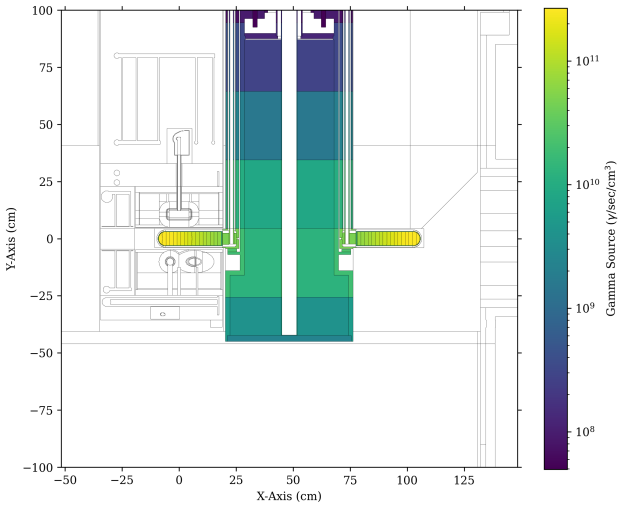


**Figure 5. Cross section view of the 1 week decay gamma source intensity for the target wedges and lower portions of the staves and shaft.**

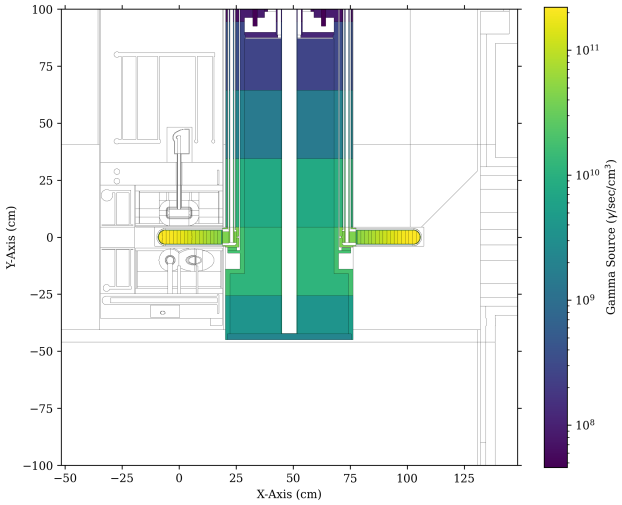


**Figure 6. Cross section view of the 2 week decay gamma source intensity for the target wedges and lower portions of the staves and shaft.**

## 6 CONCLUSIONS

Decay gamma sources for the lasagna-style target wedges and staves were calculated for 8 hours, 1 week and 2 weeks of decay after 10 years of operation. Decay gamma sources for the lasagna-style target shaft and drive were calculated for 8 hours, 1 week and 2 weeks of decay after 40 years of operation. The mechanics of the transmutation calculation beginning with the weight window calculation, and ending with the post-processing of the results is included in this report. The sources generated in this report are meant to be used as general purpose decay gamma sources for the target assembly in order to size shielding in a variety of operational configurations.

## 7 REFERENCES


[1] T. McClanahan and I. Remec, "Second Target Station High-Fidelity Target Activation Comparison," Tech. Rep. ORNL/TM-2022/2639, 2022.

[2] T. McClanahan, "Methodology to Generate the Decay Gamma Source for a Second Target Station Target Wedge," techreport ORNL/TM-2023/3210, Nov. 2023.

[3] C. J. Werner, J. Armstrong, S. G. Mashnik, G. W. McKinney, F. B. Brown, M. E. Rising, G. E. McMath, J. S. Bull, C. Solomon, J. S. Hendricks, L. Casswell, A. Sood, D. B. Pelowitz, L. J. Cox, J. E. Sweezy, R. E. Prael, D. Dixon, C. J. Werner, T. E. Booth, R. A. Forester, A. Zukaitis, M. R. James, J. T. Goorley, C. Anderson, M. L. Fensin, H. G. Hughes, J. S. Elson, T. A. Wilcox, J. Favorite, J. W. Durkee, B. C. Kiedrowski, R. Martz, and R. C. Johns, "MCNP User's Manual Code Version 6.2," Tech. Rep. LA-UR-17-29981, Oct. 2017.

[4] S. Holloway, W. Wilson, C. Kelsey, H. Little, V. Mozin, and T. England, "A Manual for CINDER2008 Codes and Data," Tech. Rep. LA-UR-11-00006, Jan. 2011.

[5] B. Micklich, F. Gallmeier, M. Wolhmuther, S. Holloway, E. Iverson, W. Lu, C. Kelsey, M. Mocko, I. Popova, and W. Wilson, "CINDER08 and scripting environment for accelerator activation problems," in *18th Topical Meeting of the Radiation Protection and Shielding Division of ANS, RPSD 2014*, pp. 355–358, 2014.

[6] M. Chadwick and et. al, "ENDF/B-VII.1 Nuclear Data for Science and Technology: Cross Sections, Covariances, Fission Product Yields and Decay Data," *Nuclear Data Sheets*, vol. 112, no. 12, pp. 2887 – 2996, 2011. Special Issue on ENDF/B-VII.1 Library.

[7] T. Miller, D. DiJulio, and V. Santoro, "Application of ADVANTG variance reduction parameters with MCNP6 at ESS," *Journal of Neutron Research*, vol. 22, pp. 199–208, 2020.

[8] I. K. Abu-Shumays, M. A. Hunter, R. L. Martz, and J. M. Risner, "Generalization of Spatial Channel Theory to Three-Dimensional x-y-z Transport Computations," Tech. Rep. DE-AC11-98PN38206, 2002.

[9] T. McClanahan, T. Goorley, and J. Auxier II, "Hiroshima and Nagasaki Verification of an Unstructured Mesh based Transmutation Toolkit," *Nuclear Technology*, pp. 1–18, 2020.

# APPENDIX A. COMPUTER HARDWARE AND SOFTWARE

# APPENDIX A. COMPUTER HARDWARE AND SOFTWARE

The Saturn cluster was used in this analysis. The mcnpmcnp6.2mod_20231005 module was used for MCNP® and cinder/2008 module was used for the AARE package.

# APPENDIX B. LOCATION OF COMPUTATIONAL INPUT AND OUTPUT FILES

# APPENDIX B. LOCATION OF COMPUTATIONAL INPUT AND OUTPUT FILES

On saturn:

CINDER2008:

/home/t25/Documents/Projects/Remote_Handling/Segment_Removal_Study/CINDER2008/Round_02/Operational_Configuration/Target

MCNP:

/home/t25/Documents/Projects/Remote_Handling/Segment_Removal_Study/MCNP/CSG/Round_02/Operational_Configuration/Calculate_Neutron_Fluxes/Target

Post-Processing:

/home/t25/Documents/Projects/Remote_Handling/Segment_Removal_Study/Post_Processing

# APPENDIX C. GEOMETRY FIGURES

# APPENDIX C. GEOMETRY FIGURES

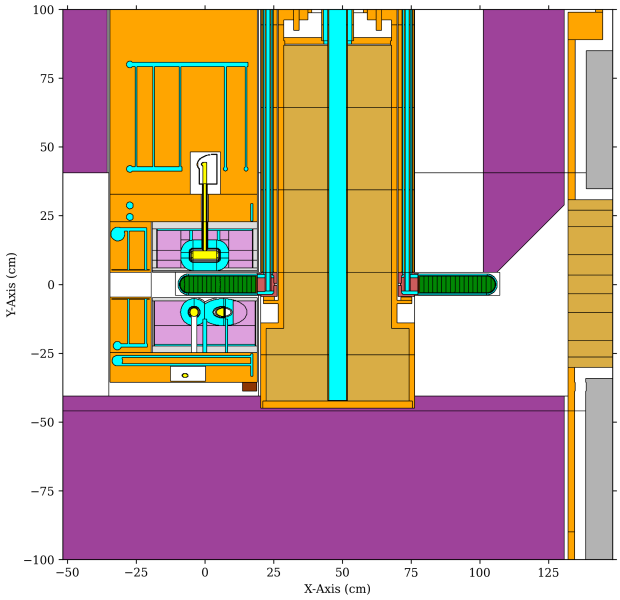


**Figure C.1. Cross section view of the target wedges and lower portions of the staves and shaft.**

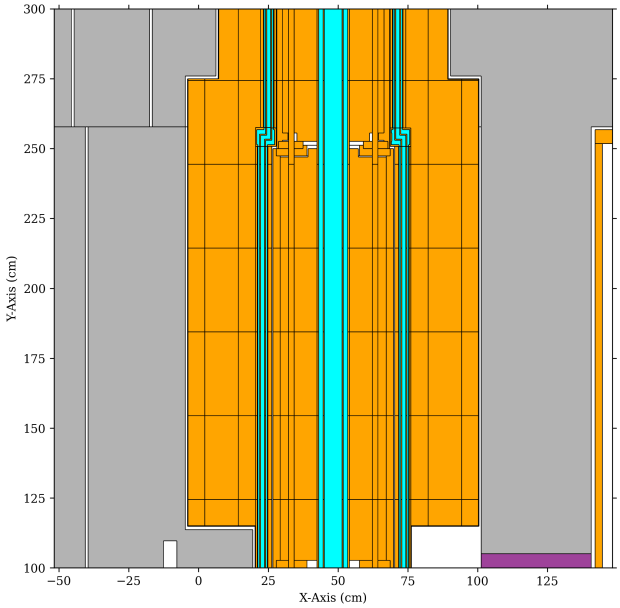


**Figure C.2. Cross section view of the target staves, donuts, and shaft.**

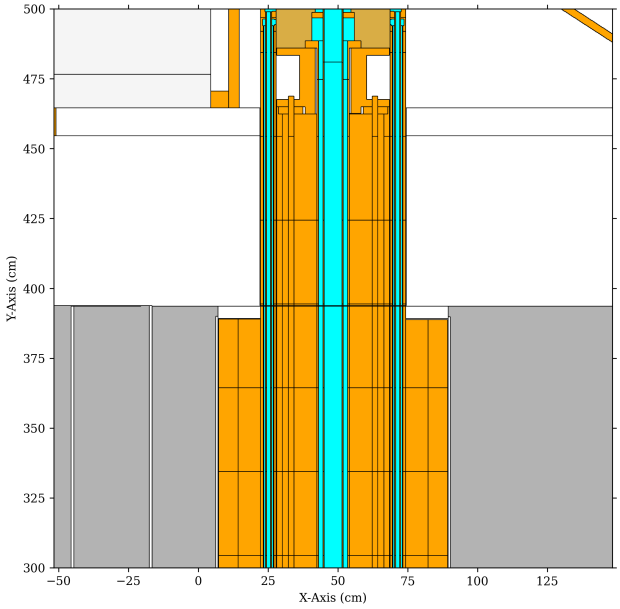


**Figure C.3. Cross section view of the target staves, shaft and lower portion of the target drive at the top of the core vessel.**

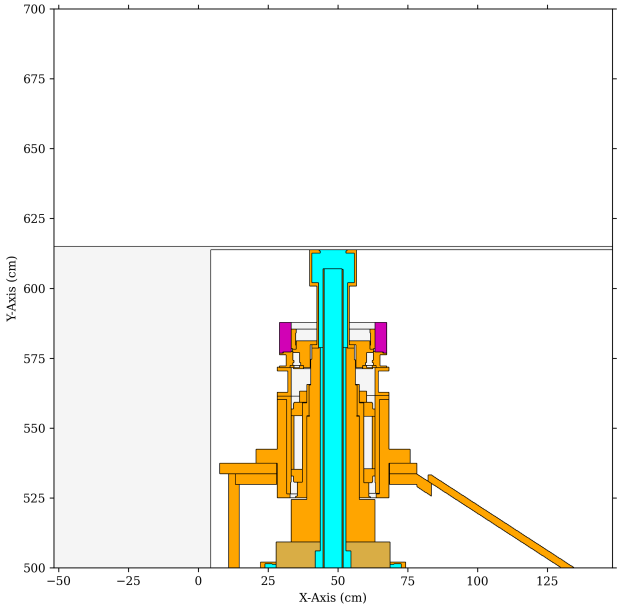


**Figure C.4. Cross section view of the top of the target drive**

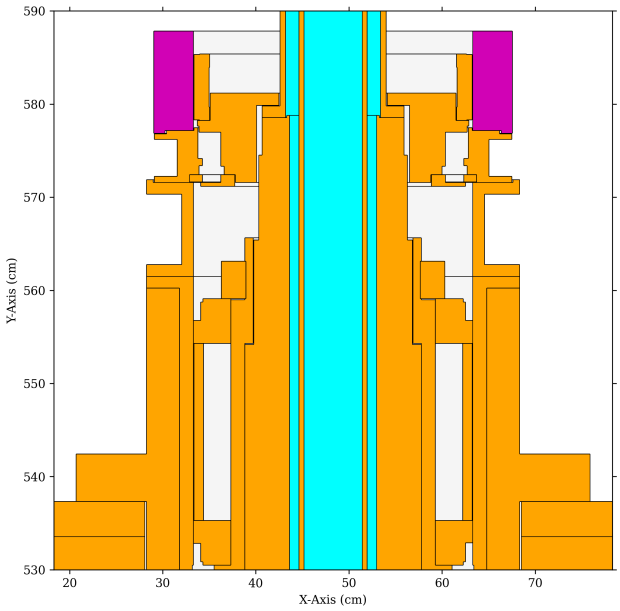


**Figure C.5. Cross section detail view of the target drive assembly.**

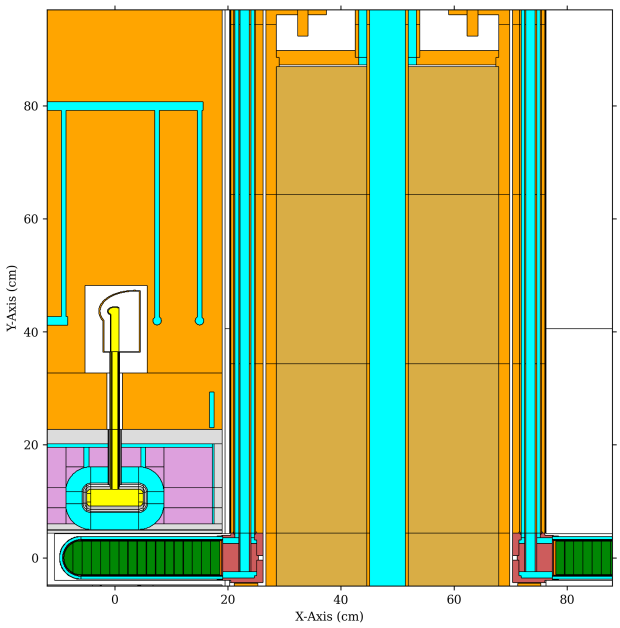


**Figure C.6. Cross section detail view of the most activated portion of the target wedges, staves, and shaft**

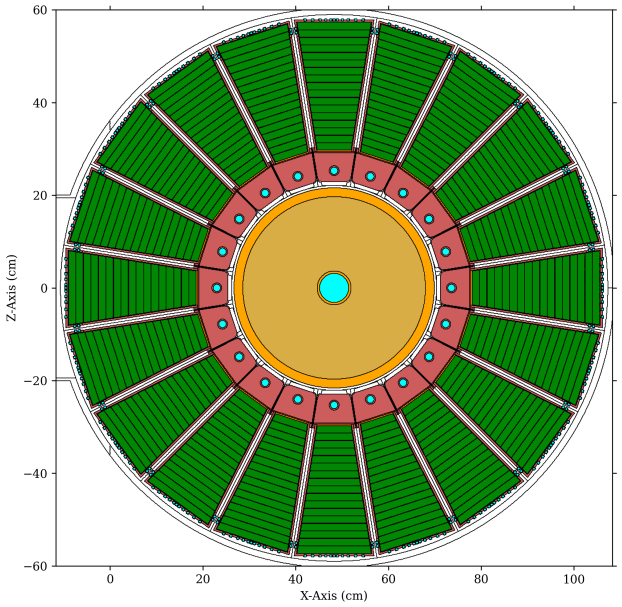


**Figure C.7. Plan view of the target wedges at beam elevation.**

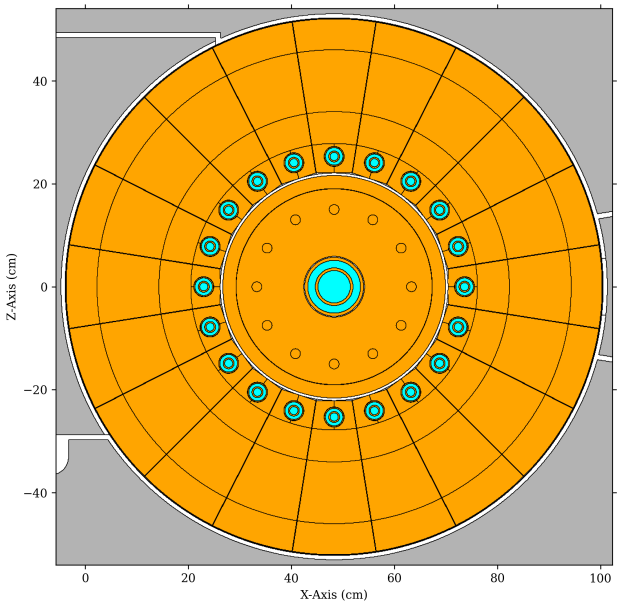


**Figure C.8. Plan view of the target staves, donut and shaft at 200 cm above the proton beam.**

# APPENDIX D. MATERIAL DEFINITIONS

# APPENDIX D. MATERIAL DEFINITIONS

**Table D.1. Tungsten Material Definition**

| Nuclide | Mass Fraction | Atom Fraction |
|---|---|---|
| $^{Nat}$C | 9.88427E-05 | 1.50586E-03 |
| $^{14}$N | 9.96107E-05 | 1.30168E-03 |
| $^{15}$N | 3.89823E-07 | 4.75547E-06 |
| $^{16}$O | 9.97297E-05 | 1.14094E-03 |
| $^{17}$O | 4.03743E-08 | 4.34609E-07 |
| $^{28}$Si | 9.18667E-05 | 6.00867E-04 |
| $^{29}$Si | 4.83364E-06 | 3.05245E-05 |
| $^{30}$Si | 3.29992E-06 | 2.01457E-05 |
| $^{54}$Fe | 5.64564E-06 | 1.91525E-05 |
| $^{56}$Fe | 9.19027E-05 | 3.00653E-04 |
| $^{57}$Fe | 2.16042E-06 | 6.94346E-06 |
| $^{58}$Fe | 2.92542E-07 | 9.24019E-07 |
| $^{58}$Ni | 6.71985E-05 | 2.12245E-04 |
| $^{60}$Ni | 2.67762E-05 | 8.17560E-05 |
| $^{61}$Ni | 1.18341E-06 | 3.55399E-06 |
| $^{62}$Ni | 3.83483E-06 | 1.13312E-05 |
| $^{64}$Ni | 1.00821E-06 | 2.88589E-06 |
| $^{180}$W | 1.17391E-03 | 1.19374E-03 |
| $^{182}$W | 2.62112E-01 | 2.63609E-01 |
| $^{183}$W | 1.42321E-01 | 1.42350E-01 |
| $^{184}$W | 3.06402E-01 | 3.04797E-01 |
| $^{186}$W | 2.87392E-01 | 2.82806E-01 |
| Density (g/cm$^3$) | 19.3 | |

**Table D.2. Tantalum Material Definition**

| Nuclide | Mass Fraction | Atom Fraction |
|---|---|---|
| $^{1}$H | 1.49987E-05 | 2.66916E-03 |
| $^{2}$H | 3.44740E-09 | 3.06983E-07 |
| $^{Nat}$C | 9.88535E-05 | 1.47610E-03 |
| $^{14}$N | 9.96216E-05 | 1.27595E-03 |
| $^{15}$N | 3.89865E-07 | 4.66149E-06 |
| $^{16}$O | 1.49607E-04 | 1.67755E-03 |
| $^{17}$O | 6.05691E-08 | 6.39040E-07 |
| $^{28}$Si | 4.59384E-05 | 2.94496E-04 |
| $^{29}$Si | 2.41708E-06 | 1.49606E-05 |
| $^{30}$Si | 1.65009E-06 | 9.87349E-06 |
| $^{46}$Ti | 7.92102E-06 | 3.09154E-05 |
| $^{47}$Ti | 7.29865E-06 | 2.78801E-05 |
| $^{48}$Ti | 7.38536E-05 | 2.76252E-04 |
| $^{49}$Ti | 5.53284E-06 | 2.02730E-05 |

**Table D.2 – continued from previous page**

| Nuclide | Mass Fraction | Atom Fraction |
|---|---|---|
| $^{50}$Ti | 5.40553E-06 | 1.94112E-05 |
| $^{54}$Fe | 5.64626E-06 | 1.87740E-05 |
| $^{56}$Fe | 9.19127E-05 | 2.94711E-04 |
| $^{57}$Fe | 2.16065E-06 | 6.80623E-06 |
| $^{58}$Fe | 2.92574E-07 | 9.05757E-07 |
| $^{58}$Ni | 6.72058E-05 | 2.08050E-04 |
| $^{60}$Ni | 2.67791E-05 | 8.01402E-05 |
| $^{61}$Ni | 1.18354E-06 | 3.48375E-06 |
| $^{62}$Ni | 3.83525E-06 | 1.11073E-05 |
| $^{64}$Ni | 1.00832E-06 | 2.82885E-06 |
| $^{93}$Nb | 1.00012E-03 | 1.93067E-03 |
| $^{92}$Mo | 2.83023E-05 | 5.52304E-05 |
| $^{94}$Mo | 1.80711E-05 | 3.45143E-05 |
| $^{95}$Mo | 3.14617E-05 | 5.94556E-05 |
| $^{96}$Mo | 3.33529E-05 | 6.23731E-05 |
| $^{97}$Mo | 1.93153E-05 | 3.57482E-05 |
| $^{98}$Mo | 4.93778E-05 | 9.04542E-05 |
| $^{100}$Mo | 2.01423E-05 | 3.61590E-05 |
| $^{181}$Ta | 9.97586E-01 | 9.88782E-01 |
| $^{180}$W | 5.87358E-07 | 5.85414E-07 |
| $^{182}$W | 1.31155E-04 | 1.29283E-04 |
| $^{183}$W | 7.12113E-05 | 6.98104E-05 |
| $^{184}$W | 1.53308E-04 | 1.49474E-04 |
| $^{186}$W | 1.43797E-04 | 1.38691E-04 |
| Density (g/cm$^3$) | 16.6 | |

**Table D.3. Copper Material Definition**

| Nuclide | Mass Fraction | Atom Fraction |
|---|---|---|
| $^{16}$O | 4.98649E-06 | 1.98105E-05 |
| $^{17}$O | 2.01869E-09 | 7.54616E-09 |
| $^{31}$P | 2.99999E-06 | 6.15472E-06 |
| $^{32}$S | 1.42070E-05 | 2.82366E-05 |
| $^{33}$S | 1.15680E-07 | 2.22947E-07 |
| $^{34}$S | 6.75338E-07 | 1.26338E-06 |
| $^{36}$S | 1.68260E-09 | 2.97274E-09 |
| $^{55}$Mn | 4.99999E-07 | 5.78333E-07 |
| $^{54}$Fe | 5.64559E-07 | 6.65094E-07 |
| $^{56}$Fe | 9.19018E-06 | 1.04405E-05 |
| $^{57}$Fe | 2.16039E-07 | 2.41120E-07 |
| $^{58}$Fe | 2.92549E-08 | 3.20888E-08 |
| $^{58}$Ni | 6.71978E-06 | 7.37044E-06 |

**Table D.3 – continued from previous page**

| Nuclide | Mass Fraction | Atom Fraction |
|---|---|---|
| $^{60}$Ni | 2.67759E-06 | 2.83907E-06 |
| $^{61}$Ni | 1.18340E-07 | 1.23417E-07 |
| $^{62}$Ni | 3.83489E-07 | 3.93501E-07 |
| $^{64}$Ni | 1.00820E-07 | 1.00216E-07 |
| $^{63}$Cu | 6.84728E-01 | 6.91425E-01 |
| $^{65}$Cu | 3.15179E-01 | 3.08467E-01 |
| $^{64}$Zn | 4.71769E-07 | 4.68935E-07 |
| $^{66}$Zn | 2.81959E-07 | 2.71776E-07 |
| $^{67}$Zn | 4.19729E-08 | 3.98519E-08 |
| $^{68}$Zn | 1.97560E-07 | 1.84821E-07 |
| $^{70}$Zn | 6.74578E-09 | 6.13027E-09 |
| $^{75}$As | 4.99999E-06 | 4.24076E-06 |
| $^{74}$Se | 2.49969E-08 | 2.14878E-08 |
| $^{76}$Se | 2.70279E-07 | 2.26226E-07 |
| $^{77}$Se | 2.22989E-07 | 1.84216E-07 |
| $^{78}$Se | 7.03688E-07 | 5.73890E-07 |
| $^{80}$Se | 1.50640E-06 | 1.19780E-06 |
| $^{82}$Se | 2.71709E-07 | 2.10773E-07 |
| $^{107}$Ag | 1.28440E-05 | 7.63454E-06 |
| $^{109}$Ag | 1.21560E-05 | 7.09292E-06 |
| $^{106}$Cd | 1.17770E-08 | 7.06632E-09 |
| $^{108}$Cd | 8.54318E-09 | 5.03110E-09 |
| $^{110}$Cd | 1.22110E-07 | 7.06029E-08 |
| $^{111}$Cd | 1.26280E-07 | 7.23548E-08 |
| $^{112}$Cd | 2.40209E-07 | 1.36405E-07 |
| $^{113}$Cd | 1.22740E-07 | 6.90806E-08 |
| $^{114}$Cd | 2.91109E-07 | 1.62406E-07 |
| $^{116}$Cd | 7.72278E-08 | 4.23404E-08 |
| $^{112}$Sn | 1.82880E-08 | 1.03848E-08 |
| $^{114}$Sn | 1.26660E-08 | 7.06620E-09 |
| $^{115}$Sn | 6.58198E-09 | 3.64004E-09 |
| $^{116}$Sn | 2.83919E-07 | 1.55664E-07 |
| $^{117}$Sn | 1.51260E-07 | 8.22204E-08 |
| $^{118}$Sn | 4.81099E-07 | 2.59296E-07 |
| $^{119}$Sn | 1.72080E-07 | 9.19639E-08 |
| $^{120}$Sn | 6.58148E-07 | 3.48802E-07 |
| $^{122}$Sn | 9.50918E-08 | 4.95689E-08 |
| $^{124}$Sn | 1.20870E-07 | 6.19883E-08 |
| $^{121}$Sb | 2.27229E-06 | 1.19428E-06 |
| $^{123}$Sb | 1.72770E-06 | 8.93269E-07 |
| $^{120}$Te | 1.69140E-09 | 8.96383E-10 |
| $^{122}$Te | 4.87219E-08 | 2.53975E-08 |
| $^{123}$Te | 1.71450E-08 | 8.86444E-09 |

**Table D.3 – continued from previous page**

| Nuclide | Mass Fraction | Atom Fraction |
|---|---|---|
| $^{124}$Te | 9.20518E-08 | 4.72099E-08 |
| $^{125}$Te | 1.38410E-07 | 7.04159E-08 |
| $^{126}$Te | 3.71779E-07 | 1.87642E-07 |
| $^{128}$Te | 6.36298E-07 | 3.16124E-07 |
| $^{130}$Te | 6.93908E-07 | 3.39433E-07 |
| $^{204}$Pb | 6.89048E-08 | 2.14664E-08 |
| $^{206}$Pb | 1.19780E-06 | 3.69532E-07 |
| $^{207}$Pb | 1.10370E-06 | 3.38854E-07 |
| $^{208}$Pb | 2.62959E-06 | 8.03445E-07 |
| $^{209}$Pb | 9.99998E-07 | 3.04071E-07 |
| Density (g/cm$^3$) | 8.93 | |

**Table D.4. Inconel-718 Material Definition**

| Nuclide | Mass Fraction | Atom Fraction |
|---|---|---|
| $^{10}$B | 1.10586E-05 | 6.35927E-05 |
| $^{11}$B | 4.89414E-05 | 2.55968E-04 |
| $^{Nat}$C | 8.00000E-04 | 3.83511E-03 |
| $^{27}$Al | 8.00000E-03 | 1.70723E-02 |
| $^{28}$Si | 3.21533E-03 | 6.61750E-03 |
| $^{29}$Si | 1.69177E-04 | 3.36174E-04 |
| $^{30}$Si | 1.15496E-04 | 2.21868E-04 |
| $^{31}$P | 1.50000E-04 | 2.78847E-04 |
| $^{32}$S | 1.42073E-04 | 2.55864E-04 |
| $^{33}$S | 1.15681E-06 | 2.02019E-06 |
| $^{34}$S | 6.75336E-06 | 1.14478E-05 |
| $^{36}$S | 1.68255E-08 | 2.69359E-08 |
| $^{46}$Ti | 9.10811E-04 | 1.14126E-03 |
| $^{47}$Ti | 8.39245E-04 | 1.02921E-03 |
| $^{48}$Ti | 8.49218E-03 | 1.01981E-02 |
| $^{49}$Ti | 6.36202E-04 | 7.48393E-04 |
| $^{50}$Ti | 6.21561E-04 | 7.16576E-04 |
| $^{50}$Cr | 8.76474E-03 | 1.01043E-02 |
| $^{52}$Cr | 1.75769E-01 | 1.94852E-01 |
| $^{53}$Cr | 2.03145E-02 | 2.20946E-02 |
| $^{54}$Cr | 5.15207E-03 | 5.49982E-03 |
| $^{55}$Mn | 3.50000E-03 | 3.66829E-03 |
| $^{54}$Fe | 6.70918E-03 | 7.16193E-03 |
| $^{56}$Fe | 1.09216E-01 | 1.12427E-01 |
| $^{57}$Fe | 2.56738E-03 | 2.59643E-03 |
| $^{58}$Fe | 3.47660E-04 | 3.45537E-04 |
| $^{59}$Co | 2.50000E-03 | 2.44258E-03 |

**Table D.4 – continued from previous page**

| Nuclide | Mass Fraction | Atom Fraction |
|---|---|---|
| $^{58}$Ni | 3.69587E-01 | 3.67318E-01 |
| $^{60}$Ni | 1.47268E-01 | 1.41490E-01 |
| $^{61}$Ni | 6.50848E-03 | 6.15049E-03 |
| $^{62}$Ni | 2.10915E-02 | 1.96104E-02 |
| $^{64}$Ni | 5.54483E-03 | 4.99420E-03 |
| $^{63}$Cu | 2.05438E-03 | 1.87973E-03 |
| $^{65}$Cu | 9.45624E-04 | 8.38603E-04 |
| $^{93}$Nb | 5.45000E-02 | 3.37769E-02 |
| $^{92}$Mo | 4.66932E-03 | 2.92533E-03 |
| $^{94}$Mo | 2.98137E-03 | 1.82808E-03 |
| $^{95}$Mo | 5.19057E-03 | 3.14913E-03 |
| $^{96}$Mo | 5.50251E-03 | 3.30362E-03 |
| $^{97}$Mo | 3.18665E-03 | 1.89344E-03 |
| $^{98}$Mo | 8.14644E-03 | 4.79104E-03 |
| $^{100}$Mo | 3.32315E-03 | 1.91523E-03 |
| $^{181}$Ta | 5.00000E-04 | 1.59105E-04 |
| Density (g/cm$^3$) | 8.19 | |

# APPENDIX E. TALLY ENERGY BINS

## APPENDIX E. TALLY ENERGY BINS

```
E04   \$ MeV
      1.000E-11 1.100E-10 3.000E-09 5.500E-09 1.000E-08 1.500E-08 2.000E-08
      3.000E-08 3.200E-08 3.238E-08 4.300E-08 5.900E-08 7.700E-08 9.500E-08
      1.000E-07 1.150E-07 1.340E-07 1.600E-07 1.890E-07 2.200E-07 2.480E-07
      2.825E-07 3.145E-07 3.520E-07 3.910E-07 4.140E-07 4.330E-07 4.850E-07
      5.316E-07 5.400E-07 6.250E-07 6.826E-07 7.050E-07 7.900E-07 8.600E-07
      8.764E-07 9.300E-07 9.860E-07 1.010E-06 1.035E-06 1.070E-06 1.080E-06
      1.090E-06 1.110E-06 1.125E-06 1.170E-06 1.235E-06 1.305E-06 1.370E-06
      1.440E-06 1.445E-06 1.510E-06 1.590E-06 1.670E-06 1.755E-06 1.840E-06
      1.855E-06 1.930E-06 2.020E-06 2.130E-06 2.360E-06 2.372E-06 2.768E-06
      3.059E-06 3.381E-06 3.928E-06 4.129E-06 4.470E-06 4.670E-06 5.043E-06
      5.623E-06 6.160E-06 6.476E-06 7.079E-06 7.524E-06 7.943E-06 8.315E-06
      8.913E-06 9.190E-06 1.000E-05 1.068E-05 1.122E-05 1.259E-05 1.371E-05
      1.523E-05 1.674E-05 1.760E-05 1.903E-05 2.045E-05 2.260E-05 2.498E-05
      2.792E-05 2.920E-05 3.051E-05 3.389E-05 3.727E-05 3.981E-05 4.552E-05
      4.785E-05 5.012E-05 5.559E-05 6.144E-05 6.310E-05 6.790E-05 7.079E-05
      7.889E-05 8.528E-05 9.166E-05 1.013E-04 1.122E-04 1.301E-04 1.367E-04
      1.585E-04 1.670E-04 1.778E-04 2.040E-04 2.145E-04 2.430E-04 2.754E-04
      3.043E-04 3.536E-04 3.981E-04 4.540E-04 5.145E-04 5.830E-04 6.310E-04
      6.773E-04 7.079E-04 7.485E-04 8.482E-04 9.611E-04 1.010E-03 1.117E-03
      1.234E-03 1.364E-03 1.507E-03 1.585E-03 1.796E-03 2.035E-03 2.113E-03
      2.249E-03 2.371E-03 2.485E-03 2.613E-03 2.661E-03 2.747E-03 2.818E-03
      3.035E-03 3.162E-03 3.355E-03 3.548E-03 3.707E-03 3.981E-03 4.307E-03
      4.643E-03 5.004E-03 5.531E-03 6.267E-03 7.102E-03 7.466E-03 8.251E-03
      9.119E-03 1.008E-02 1.114E-02 1.171E-02 1.273E-02 1.383E-02 1.503E-02
      1.585E-02 1.662E-02 1.778E-02 1.931E-02 1.995E-02 2.054E-02 2.113E-02
      2.187E-02 2.239E-02 2.304E-02 2.358E-02 2.418E-02 2.441E-02 2.479E-02
      2.512E-02 2.585E-02 2.606E-02 2.661E-02 2.700E-02 2.738E-02 2.818E-02
      2.850E-02 2.901E-02 2.985E-02 3.073E-02 3.162E-02 3.183E-02 3.431E-02
      3.698E-02 4.087E-02 4.359E-02 4.631E-02 4.939E-02 5.248E-02 5.517E-02
      5.656E-02 6.173E-02 6.738E-02 7.200E-02 7.499E-02 7.950E-02 8.230E-02
      8.250E-02 8.652E-02 9.804E-02 1.111E-01 1.168E-01 1.228E-01 1.291E-01
      1.357E-01 1.426E-01 1.500E-01 1.576E-01 1.657E-01 1.742E-01 1.832E-01
      1.925E-01 2.024E-01 2.128E-01 2.237E-01 2.352E-01 2.472E-01 2.732E-01
      2.873E-01 2.945E-01 2.972E-01 2.985E-01 3.020E-01 3.337E-01 3.688E-01
      3.877E-01 4.076E-01 4.505E-01 5.234E-01 5.502E-01 5.784E-01 6.081E-01
      6.393E-01 6.721E-01 7.065E-01 7.427E-01 7.808E-01 8.209E-01 8.629E-01
      9.072E-01 9.616E-01 1.003E+00 1.108E+00 1.165E+00 1.225E+00 1.287E+00
      1.353E+00 1.423E+00 1.496E+00 1.572E+00 1.653E+00 1.738E+00 1.827E+00
      1.921E+00 2.019E+00 2.122E+00 2.231E+00 2.307E+00 2.346E+00 2.365E+00
      2.385E+00 2.466E+00 2.592E+00 2.725E+00 2.865E+00 3.012E+00 3.166E+00
      3.329E+00 3.679E+00 4.066E+00 4.493E+00 4.724E+00 4.966E+00 5.220E+00
      5.488E+00 5.769E+00 6.065E+00 6.376E+00 6.592E+00 6.703E+00 7.047E+00
      7.408E+00 7.788E+00 8.187E+00 8.607E+00 9.048E+00 9.512E+00 1.000E+01
      1.051E+01 1.105E+01 1.162E+01 1.221E+01 1.284E+01 1.350E+01 1.384E+01
      1.419E+01 1.455E+01 1.492E+01 1.568E+01 1.649E+01 1.691E+01 1.733E+01
      1.964E+01 2.000E+01
```

# APPENDIX F. GAMMA SOURCE FIGURES

# APPENDIX F. GAMMA SOURCE FIGURES

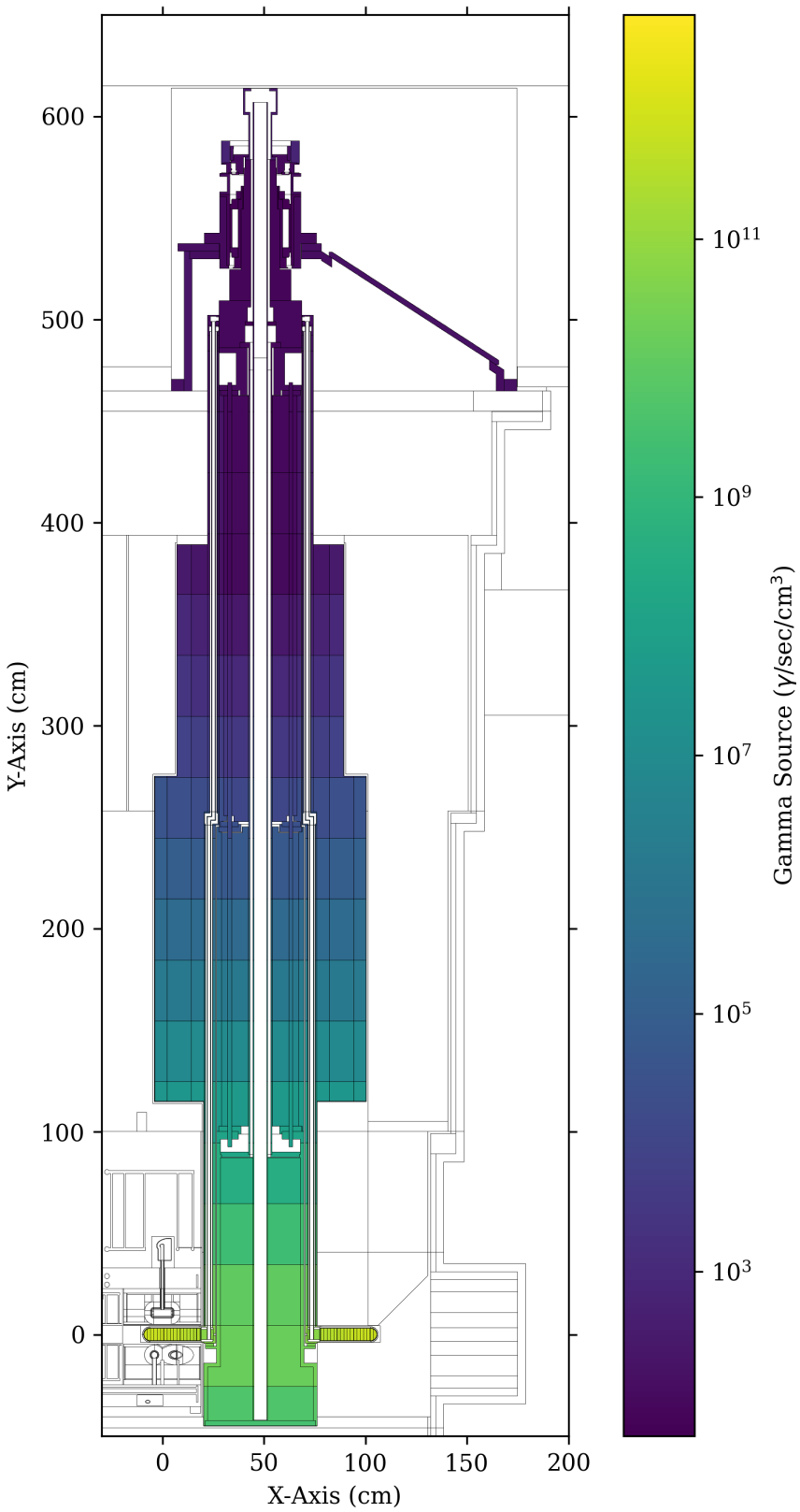


**Figure F.1. Cross section view of the 8 hour decay gamma source intensity for the full target target assembly.**

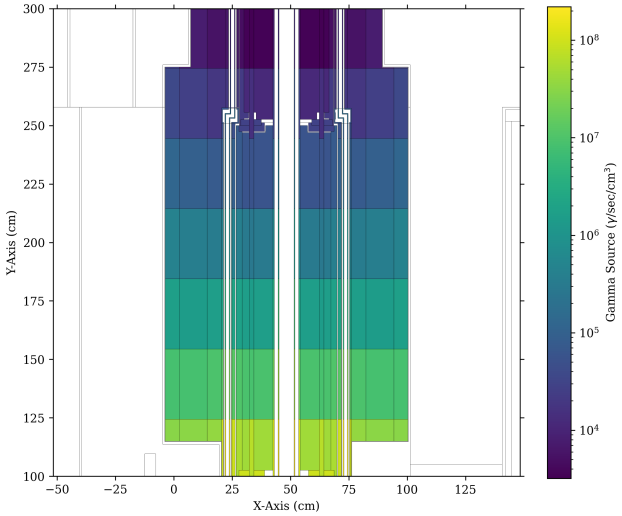


**Figure F.2. Cross section view of the 8 hour decay gamma source intensity for the target staves, donuts, and shaft.**

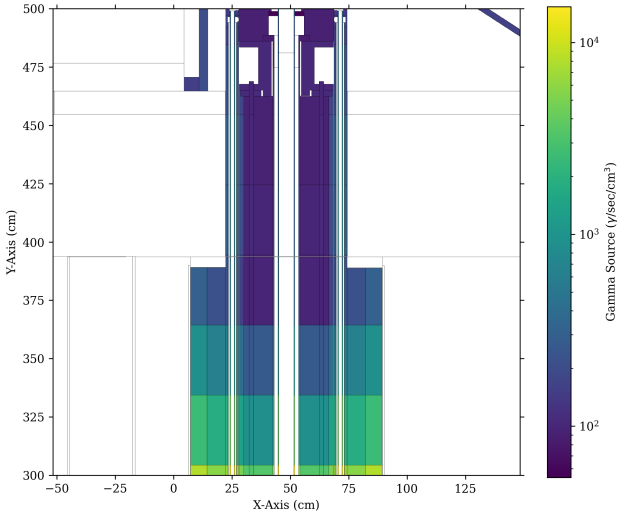


**Figure F.3. Cross section view of the 8 hour decay gamma source intensity at the top of the core vessel shielding for the target staves, shaft and lower portion of the target drive.**

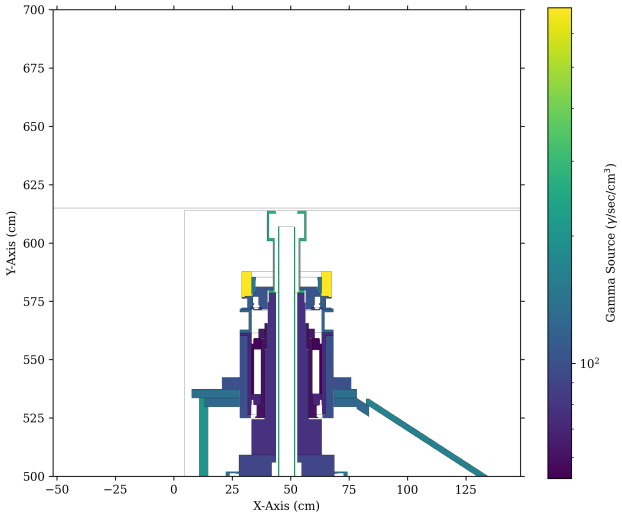


**Figure F.4. Cross section view of the 8 hour decay gamma source intensity for the top of the target drive.**

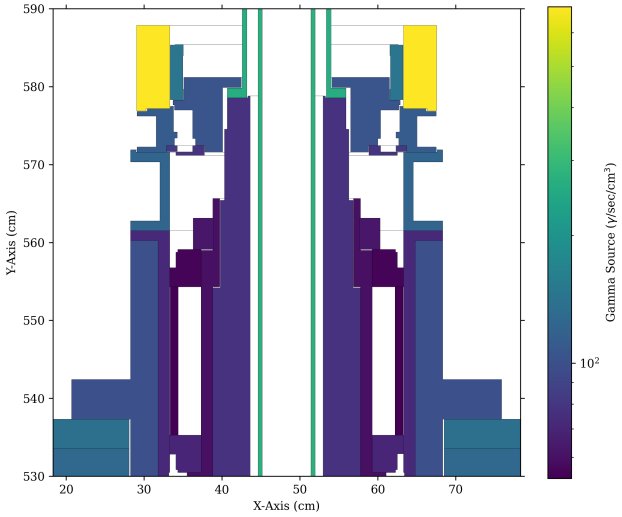


**Figure F.5. Cross section detail view of the 8 hour decay gamma source intensity for the target drive assembly where the copper motor is the most activated.**

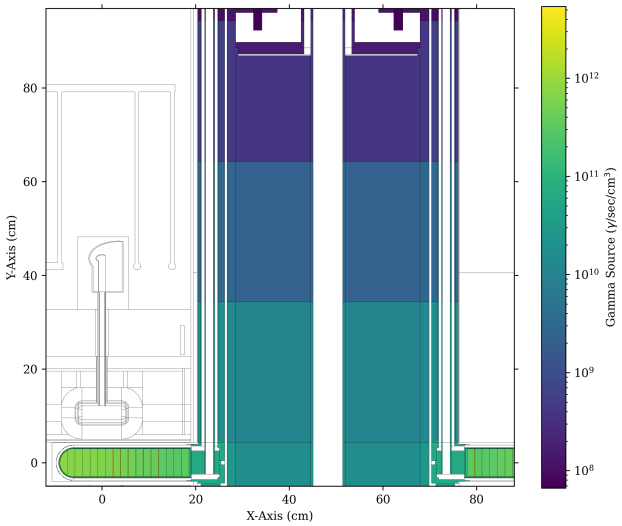


**Figure F.6. Cross section detail view of the 8 hour decay gamma source intensity for the most activated portion of the target wedges, staves, and shaft.**

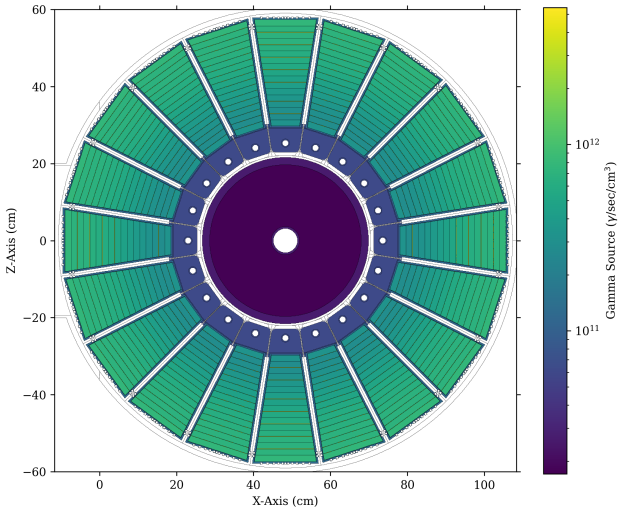


**Figure F.7. Plan view of the target wedges at beam elevation for the 8 hour decay gamma source term.**

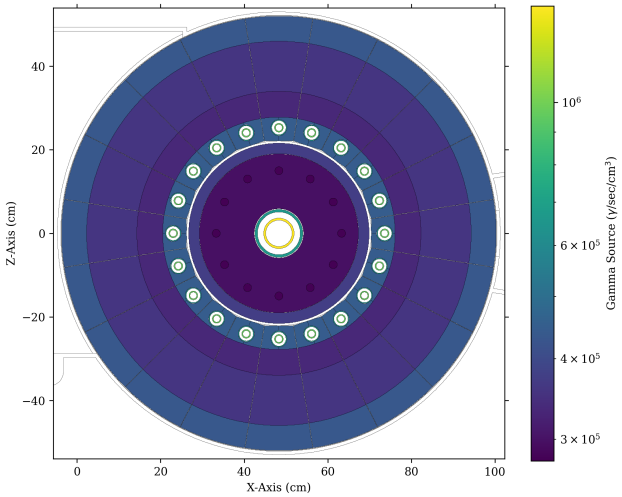


**Figure F.8. Plan view of the target staves, donut and shaft at 200 cm above the proton beam for the 8 hour decay gamma source term.**

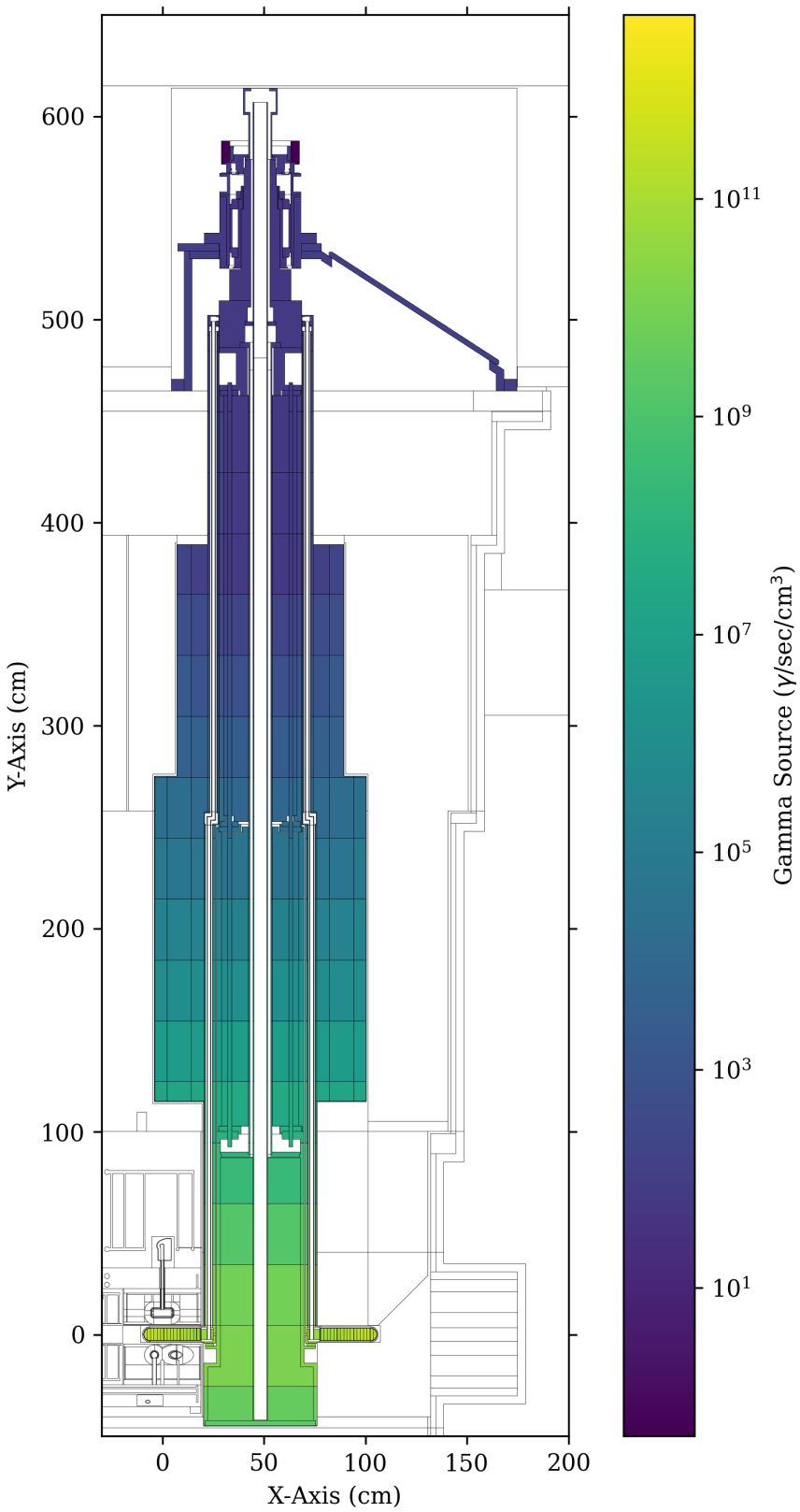


**Figure F.9. Cross section view of the 1 week decay gamma source intensity for the full target target assembly.**

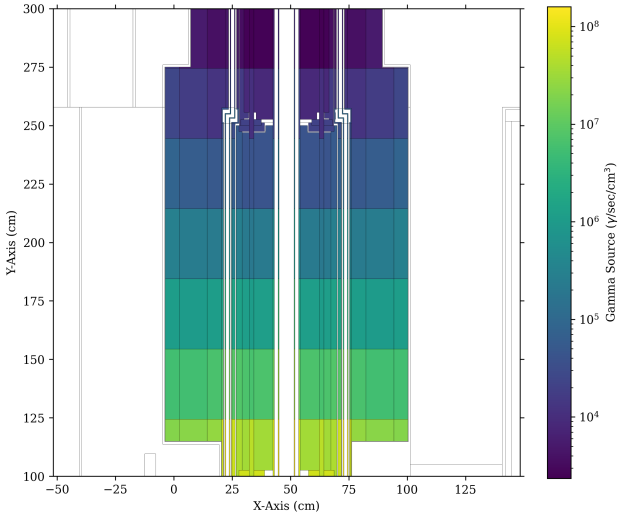


**Figure F.10. Cross section view of the 1 week decay gamma source intensity for the target staves, donuts, and shaft.**

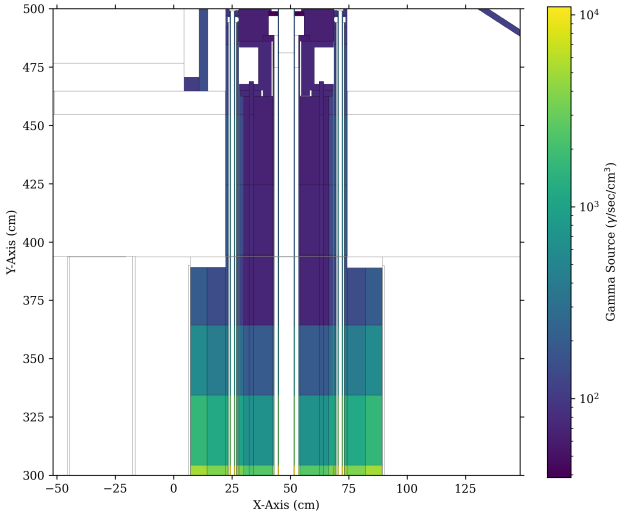


**Figure F.11. Cross section view of the 1 week decay gamma source intensity at the top of the core vessel shielding for the target staves, shaft and lower portion of the target drive.**

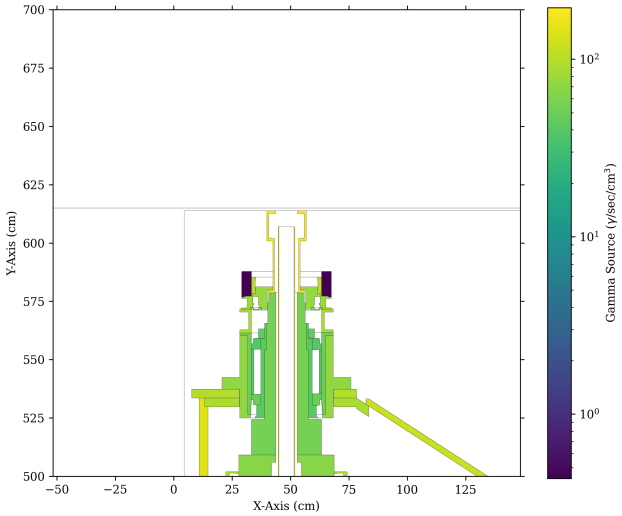


**Figure F.12. Cross section view of the 1 week decay gamma source intensity for the top of the target drive.**

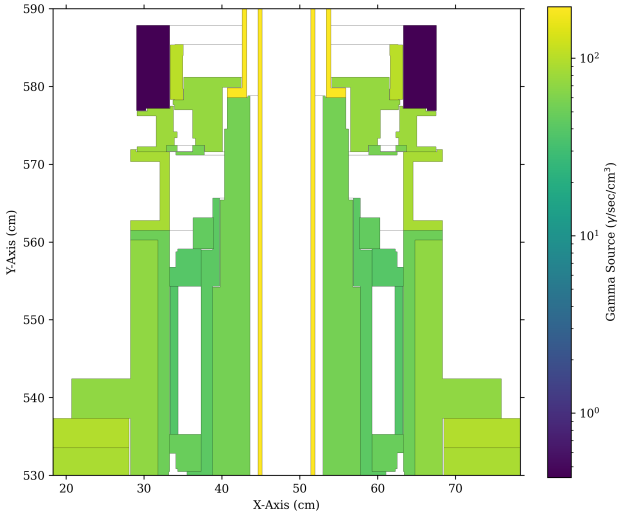


**Figure F.13. Cross section detail view of the 1 week decay gamma source intensity for the target drive assembly.**

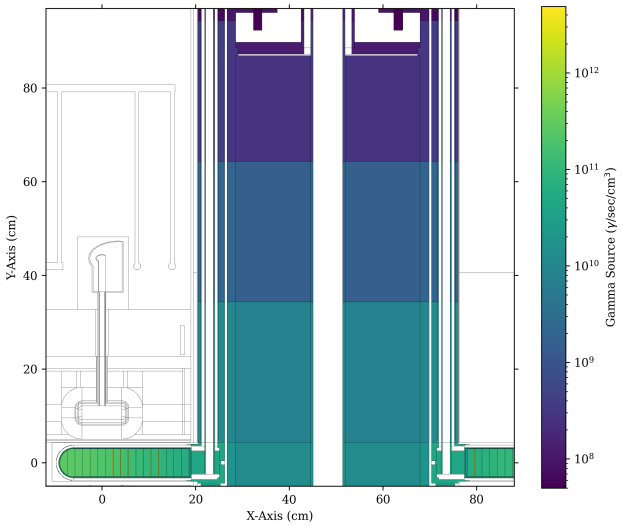


**Figure F.14. Cross section detail view of the 1 week decay gamma source intensity for the most activated portion of the target wedges, staves, and shaft.**

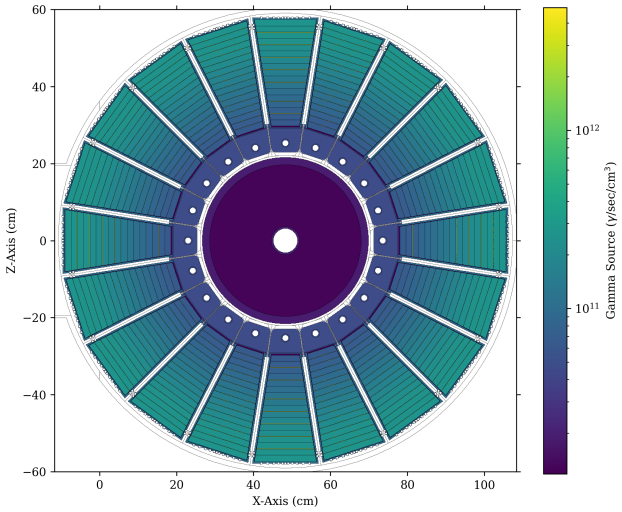


**Figure F.15. Plan view of the target wedges at beam elevation for the 1 week decay gamma source term.**

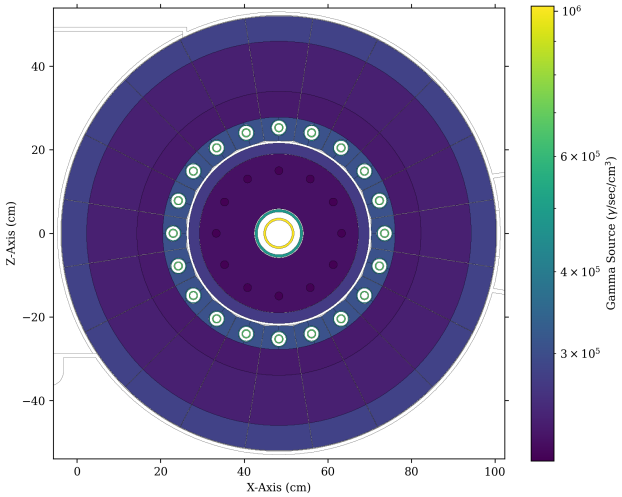


**Figure F.16. Plan view of the target staves, donut and shaft at 200 cm above the proton beam for the 1 week decay gamma source term.**

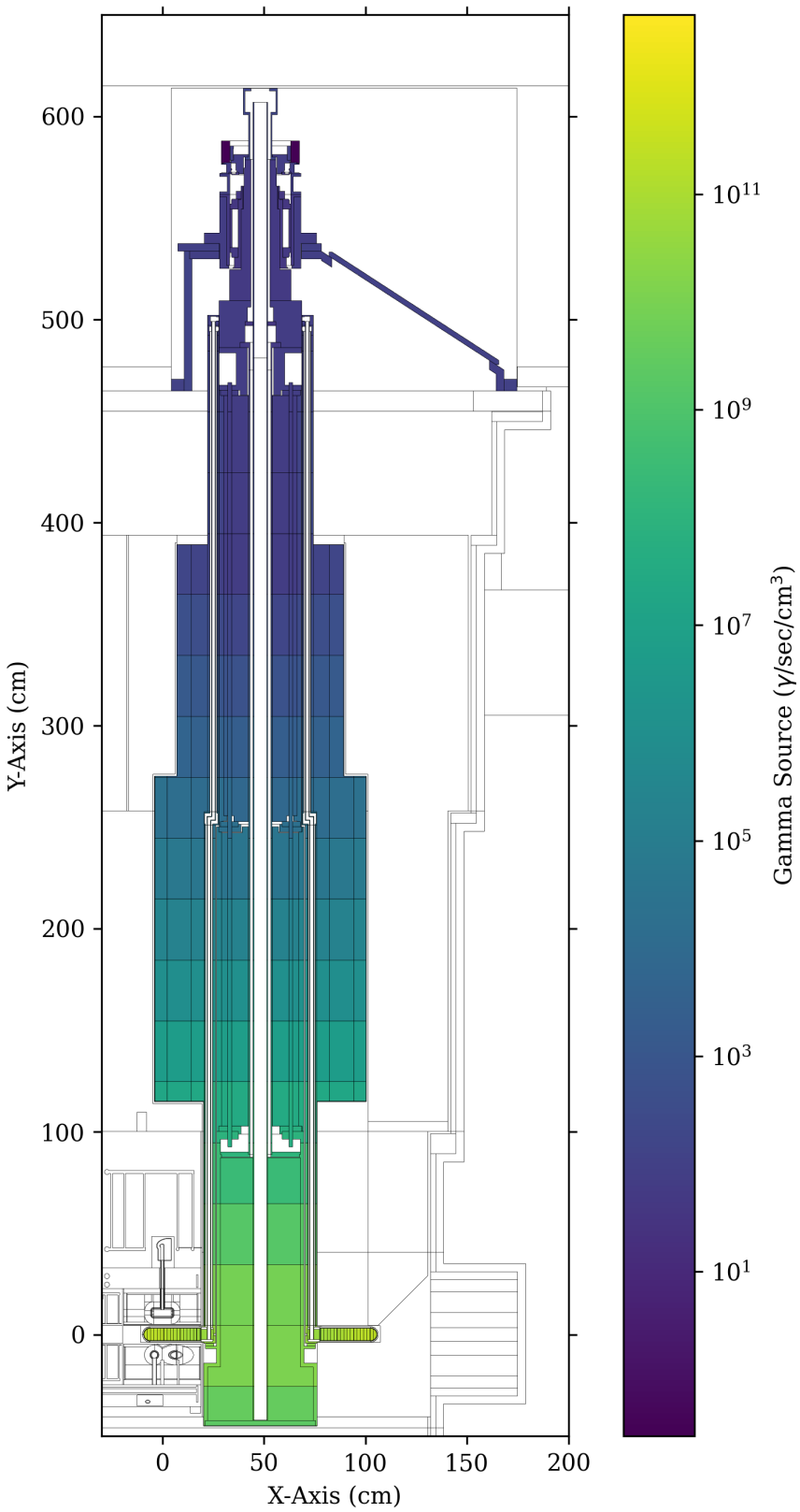


**Figure F.17. Cross section view of the 2 week decay gamma source intensity for the full target target assembly.**

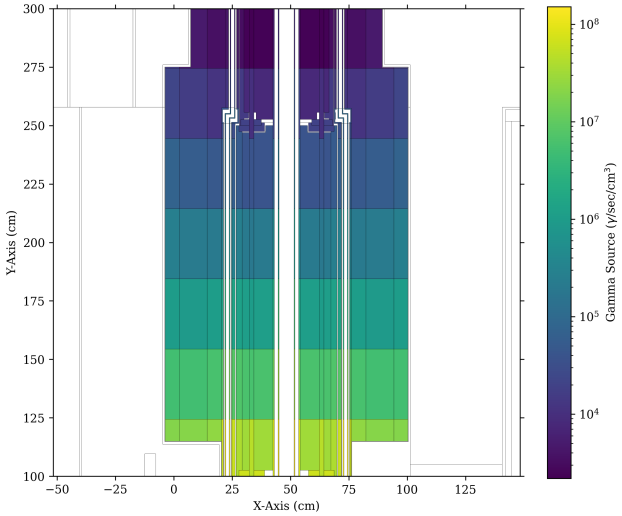


**Figure F.18. Cross section view of the 2 week decay gamma source intensity for the target staves, donuts, and shaft.**

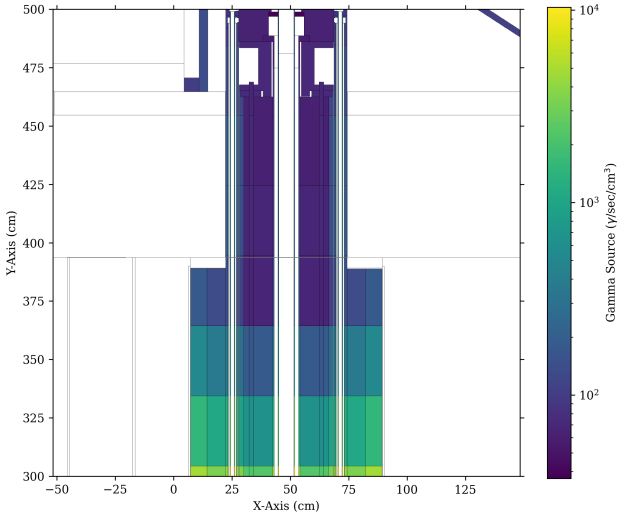


**Figure F.19. Cross section view of the 2 week decay gamma source intensity at the top of the core vessel shielding for the target staves, shaft and lower portion of the target drive.**

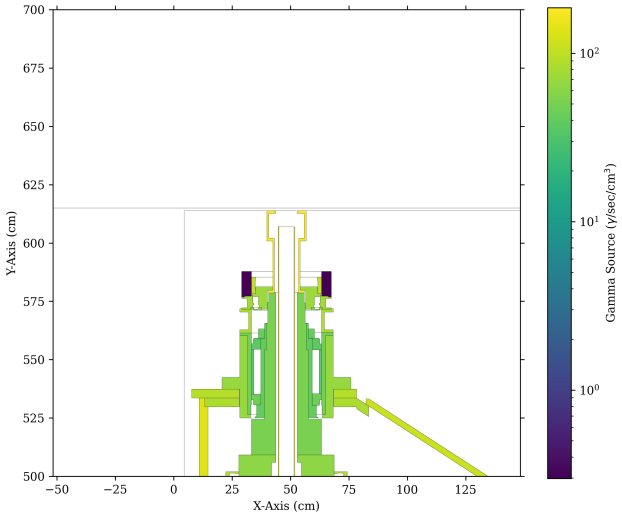


**Figure F.20. Cross section view of the 2 week decay gamma source intensity for the top of the target drive.**

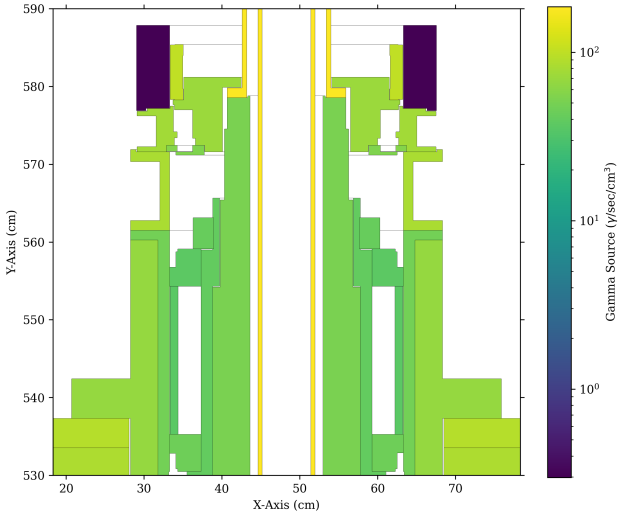


**Figure F.21. Cross section detail view of the 2 week decay gamma source intensity for the target drive assembly.**

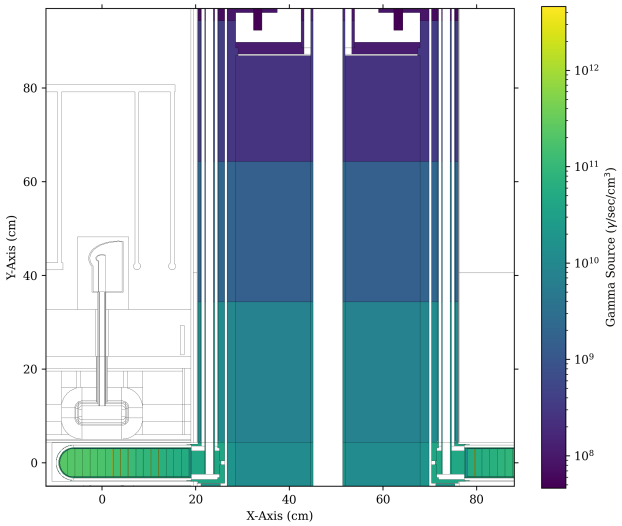


**Figure F.22. Cross section detail view of the 2 week decay gamma source intensity for the most activated portion of the target wedges, staves, and shaft.**

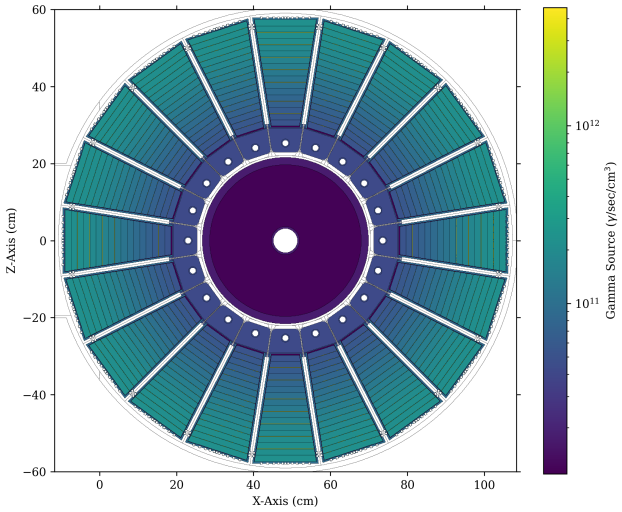


**Figure F.23. Plan view of the target wedges at beam elevation for the 2 week decay gamma source term.**

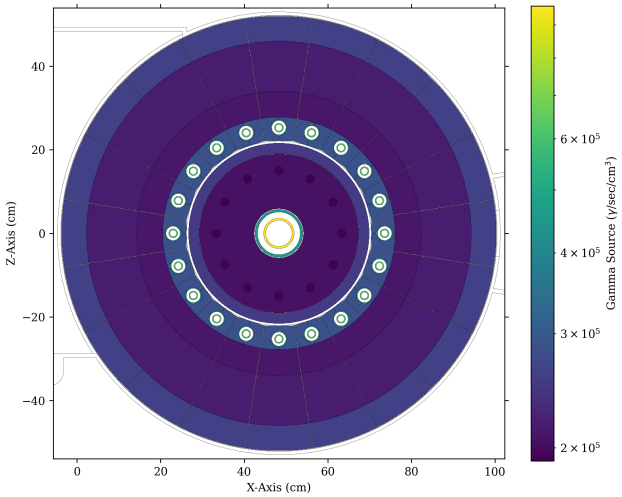


**Figure F.24. Plan view of the target staves, donut and shaft at 200 cm above the proton beam for the 2 week decay gamma source term.**